













TECH BRIEFS

NATIONAL AERONAUTICS AND SPACE ADMINISTRATION

-  Technology Focus
-  Electronics/Computers
-  Software
-  Materials
-  Mechanics/Machinery
-  Manufacturing
-  Bio-Medical
-  Physical Sciences
-  Information Sciences
-  Books and Reports
-  Green Design

INTRODUCTION

Tech Briefs are short announcements of innovations originating from research and development activities of the National Aeronautics and Space Administration. They emphasize information considered likely to be transferable across industrial, regional, or disciplinary lines and are issued to encourage commercial application.

Availability of NASA Tech Briefs and TSPs

Requests for individual Tech Briefs or for Technical Support Packages (TSPs) announced herein should be addressed to

National Technology Transfer Center

Telephone No. **(800) 678-6882** or via World Wide Web at **www.nttc.edu**

Please reference the control numbers appearing at the end of each Tech Brief. Information on NASA's Innovative Partnerships Program (IPP), its documents, and services is also available at the same facility or on the World Wide Web at **<http://www.nasa.gov/offices/ipp/network/index.html>**

Innovative Partnerships Offices are located at NASA field centers to provide technology-transfer access to industrial users. Inquiries can be made by contacting NASA field centers listed below.

Ames Research Center
Mary Walsh
(650) 604-1405
mary.w.walsh@nasa.gov

Dryden Flight Research Center
Yvonne D. Gibbs
(661) 276-3720
yvonne.d.gibbs@nasa.gov

Glenn Research Center
Joe Shaw, Acting Chief
(216) 977-7135
robert.j.shaw@nasa.gov

Goddard Space Flight Center
Nona Cheeks
(301) 286-5810
nona.k.cheeks@nasa.gov

Jet Propulsion Laboratory
Indrani Graczyk
(818) 354-2241
indrani.graczyk@jpl.nasa.gov

Johnson Space Center
information
(281) 483-3809
jsc.techtran@mail.nasa.gov

Kennedy Space Center
David R. Makufka
(321) 867-6227
david.r.makufka@nasa.gov

Langley Research Center
Elizabeth B. Plentovich
(757) 864-2857
elizabeth.b.plentovich@nasa.gov

Marshall Space Flight Center
Jim Dowdy
(256) 544-7604
jim.dowdy@msfc.nasa.gov

Stennis Space Center
Ramona Travis
(228) 688-3832
ramona.e.travis@nasa.gov

Carl Ray, Program Executive
Small Business Innovation
Research (SBIR) & Small
Business Technology
Transfer (STTR) Programs
(202) 358-4652
carl.g.ray@nasa.gov

Doug Comstock, Partnerships
Innovation and Commercial
Space Program Office (formerly IPP)
(202) 358-2221
doug.comstock@nasa.gov



TECH BRIEFS

NATIONAL AERONAUTICS AND SPACE ADMINISTRATION



5 Technology Focus: Test & Measurement

- 5 Multi-Segment Radius Measurement Using an Absolute Distance Meter Through a Null Assembly
- 5 Fiber-Optic Magnetic-Field-Strength Measurement System for Lightning Detection
- 6 Photocatalytic Active Radiation Measurements and Use
- 6 Computer Generated Hologram System for Wavefront Measurement System Calibration
- 7 Non-Contact Thermal Properties Measurement With Low-Power Laser and IR Camera System



9 Electronics/Computers

- 9 SpaceCube 2.0: An Advanced Hybrid Onboard Data Processor
- 9 CMOS Imager Has Better Cross-Talk and Full-Well Performance
- 10 High-Performance Wireless Telemetry
- 11 Telemetry-Based Ranging



13 Software

- 13 JWST Wavefront Control Toolbox
- 13 Java Image I/O for VICAR, PDS, and ISIS
- 13 X-Band Acquisition Aid Software



15 Manufacturing & Prototyping

- 15 Antimicrobial-Coated Granules for Disinfecting Water
- 15 Range 7 Scanner Integration With PaR Robot Scanning System
- 15 Methods of Antimicrobial Coating of Diverse Materials
- 16 High-Operating-Temperature Barrier Infrared Detector With Tailorable Cutoff Wavelength



17 Materials & Coatings

- 17 A Model of Reduced Kinetics for Alkane Oxidation Using Constituents and Species for N-Heptane
- 17 Thermally Conductive Tape Based on Carbon Nanotube Arrays
- 18 Two Catalysts for Selective Oxidation of Contaminant Gases
- 18 Nanoscale Metal Oxide Semiconductors for Gas Sensing
- 19 Lightweight, Ultra-High-Temperature, CMC-Lined Carbon/Carbon Structures



21 Mechanics/Machinery

- 21 Sample Acquisition and Handling System From a Remote Platform
- 22 Improved Rare-Earth Emitter Hollow Cathode
- 22 High-Temperature Smart Structures for Engine Noise Reduction and Performance Enhancement
- 23 Cryogenic Scan Mechanism for Fourier Transform Spectrometer
- 23 Piezoelectric Rotary Tube Motor



25 Green Design

- 25 Thermoelectric Energy Conversion Technology for High-Altitude Airships
- 25 Combustor Computations for CO₂-Neutral Aviation



27 Physical Sciences

- 27 Use of Dynamic Distortion to Predict and Alleviate Loss of Control
- 27 Cycle Time Reduction in Trapped Mercury Ion Atomic Frequency Standards
- 28 A ²⁰¹Hg⁺ Comagnetometer for ¹⁹⁹Hg⁺ Trapped Ion Space Atomic Clocks

This document was prepared under the sponsorship of the National Aeronautics and Space Administration. Neither the United States Government nor any person acting on behalf of the United States Government assumes any liability resulting from the use of the information contained in this document, or warrants that such use will be free from privately owned rights.



Multi-Segment Radius Measurement Using an Absolute Distance Meter Through a Null Assembly

This system can be used by fabricators or optics integrators for telescopes or other imaging systems.

NASA's Goddard Space Flight Center, Greenbelt, MD

This system was one of the test methods considered for measuring the radius of curvature of one or more of the 18 segmented mirrors that form the 6.5 m diameter primary mirror (PM) of the James Webb Space Telescope (JWST). The assembled telescope will be tested at cryogenic temperatures in a 17-m diameter by 27-m high vacuum chamber at the Johnson Space Center. This system uses a Leica Absolute Distance Meter (ADM), at a wavelength of 780 nm, combined with beam-steering and beam-shaping optics to make a differential distance measurement between a ring mirror on the reflective null assembly and individual PM segments. The ADM is located inside the same Pressure-Tight Enclosure (PTE) that houses the test interferometer. The PTE maintains the ADM and interferometer at ambient temperature and pressure so that they are not directly exposed to the telescope's harsh cryogenic and vacuum environment.

This system takes advantage of the existing achromatic objective and reflective null assembly used by the test interferometer to direct four ADM beamlets

to four PM segments through an optical path that is coincident with the interferometer beam. A mask, positioned on a linear slide, contains an array of 1.25 mm diameter circular subapertures that map to each of the 18 PM segments as well as six positions around the ring mirror. A down-collimated 4 mm ADM beam simultaneously covers 4 adjacent PM segment beamlets and one ring mirror beamlet. The radius, or spacing, of all 18 segments can be measured with the addition of two orthogonally-oriented scanning pentaprisms used to steer the ADM beam to any one of six different sub-aperture configurations at the plane of the ring mirror.

The interferometer beam, at a wavelength of 687 nm, and the ADM beamlets, at a wavelength of 780 nm, pass through the objective and null so that the rays are normally incident on the parabolic PM surface. After reflecting off the PM, both the ADM and interferometer beams return to their respective instruments on nearly the same path. A fifth beamlet, acting as a differential reference, reflects off a ring mirror at-

tached to the objective and null and returns to the ADM. The spacings between the ring mirror, objective, and null are known through manufacturing tolerances as well as through an *in situ* null wavefront alignment of the interferometer test beam with a reflective hologram located near the caustic of the null. Since total path length between the ring mirror and PM segments is highly deterministic, any ADM-measured departures from the predicted path length can be attributed to either spacing error or radius error in the PM. It is estimated that the path length measurement between the ring mirror and a PM segment is accurate to better than 100 μm .

The unique features of this invention include the differential distance measuring capability and its integration into an existing cryogenic and vacuum compatible interferometric optical test.

This work was done by Cormic Merle, Eric Wick, and Joseph Hayden of ITT Corp. for Goddard Space Flight Center. For further information, contact the Goddard Innovative Partnerships Office at (301) 286-5810. GSC-15674-1

Fiber-Optic Magnetic-Field-Strength Measurement System for Lightning Detection

Fiber optics used for signal paths provide enhanced immunity from electromagnetic radiation incident in the vicinity of the measurements.

John F. Kennedy Space Center, Florida

A fiber-optic sensor system is designed to measure magnetic fields associated with a lightning stroke. Field vector magnitudes are detected and processed for multiple locations. Since physical limitations prevent the sensor elements from being located in close proximity to highly conductive materials such as aluminum, the copper wire sensor elements (3) are located inside a

4-cubic-in. (≈ 66 -cubic-cm) plastic housing sensor head and connected to a fiber-optic conversion module by shielded cabling, which is limited to the shortest length feasible. The signal path between the conversion module and the avionics unit which processes the signals are fiber optic, providing enhanced immunity from electromagnetic radiation incident in the vicinity

of the measurements. The sensors are passive, lightweight, and much smaller than commercial B-dot sensors in the configuration which measures a three-dimensional magnetic field. The system is expandable, and provides a standard-format output signal for downstream processing.

Inside of the sensor head, three small search coils, each having a few

turns on a circular form, are mounted orthogonally inside the non-metallic housing. The fiber-optic conversion module comprises three interferometers, one for each search coil. Each interferometer has a high bandwidth optical phase modulator that impresses the signal received from its search coil onto its output. The output of each interferometer travels by fiber optic cable to the avionics unit, and the search coil signal is recovered by an optical phase demodulator. The output of each demodulator is fed to an

analog-to-digital converter, whose sampling rate is determined by the maximum expected rate of rise and peak signal magnitude. The output of the digital processor is a faithful reproduction of the coil response to the incident magnetic field. This information is provided in a standard output format on a 50-ohm port that can be connected to any number of data collection and processing instruments and/or systems.

The measurement of magnetic fields using fiber-optic signal processing is

novel because it eliminates limitations of a traditional B-dot system. These limitations include the distance from the sensor to the measurement device, the potential for the signal to degrade or be corrupted by EMI from lightning, and the size and weight of the sensor and associated plate.

This work was done by Jay Gurecki of Kennedy Space Center; Bob Scully of Johnson Space Center; and Allen Davis, Clay Kirkendall, and Frank Bucholtz of the Naval Research Laboratory. Further information is contained in a TSP (see page 1). KSC-13221

Photocatalytic Active Radiation Measurements and Use

This technology can be used to improve the ability to predict the performance of photocatalytic materials under different illumination conditions.

Stennis Space Center, Mississippi

Photocatalytic materials are being used to purify air, to kill microbes, and to keep surfaces clean. A wide variety of materials are being developed, many of which have different abilities to absorb various wavelengths of light. Material variability, combined with both spectral illumination intensity and spectral distribution variability, will produce a wide range of performance results. The proposed technology estimates photocatalytic active radiation (PcAR), a unit of radiation that normalizes the amount of light based on its spectral distribution and on the ability of the material to absorb that radiation.

Photocatalytic reactions depend upon the number of electron-hole pairs generated at the photocatalytic surface. The number of electron-hole pairs produced depends on the number of photons per unit area per second striking the surface that can be absorbed and whose energy exceeds the bandgap of the photocatalytic material. A convenient parameter to describe the number of useful pho-

tons is the number of moles of photons striking the surface per unit area per second. The unit of micro-einsteins (or micromoles) of photons per m² per sec is commonly used for photochemical and photoelectric-like phenomena. This type of parameter is used in photochemistry, such as in the conversion of light energy for photosynthesis.

Photosynthetic response correlates with the number of photons rather than by energy because, in this photochemical process, each molecule is activated by the absorption of one photon. In photosynthesis, the number of photons absorbed in the 400–700 nm spectral range is estimated and is referred to as photosynthetic active radiation (PAR). PAR is defined in terms of the photosynthetic photon flux density measured in micro-einsteins of photons per m² per sec. PcAR is an equivalent, similarly modeled parameter that has been defined for the photocatalytic processes.

Two methods to measure the PcAR level are being proposed. In the first

method, a calibrated spectrometer with a cosine receptor is used to measure the spectral irradiance. This measurement, in conjunction with the photocatalytic response as a function of wavelength, is used to estimate the PcAR. The photocatalytic response function is determined by measuring photocatalytic reactivity as a function of wavelength. In the second method, simple shaped photocatalytic response functions can be simulated with a broad-band detector with a cosine receptor appropriately filtered to represent the spectral response of the photocatalytic material. This second method can be less expensive than using a calibrated spectrometer.

This work was done by Bruce A. Davis of Stennis Space Center and Robert E. Ryan and Lauren W. Underwood of Science Systems and Applications, Inc. Inquiries concerning the technology should be addressed to the Intellectual Property Manager, Stennis Space Center, (228) 688-1929. Refer to SSC-00328.

Computer Generated Hologram System for Wavefront Measurement System Calibration

NASA's Goddard Space Flight Center, Greenbelt, Maryland

Computer Generated Holograms (CGHs) have been used for some time to calibrate interferometers that require nulling optics. A typical scenario is the testing of aspheric surfaces with

an interferometer placed near the paraxial center of curvature. Existing CGH technology suffers from a reduced capacity to calibrate middle and high spatial frequencies. The root

cause of this shortcoming is as follows: the CGH is not placed at an image conjugate of the asphere due to limitations imposed by the geometry of the test and the allowable size of the CGH.

This innovation provides a calibration system where the imaging properties in calibration can be made comparable to the test configuration. Thus, if the test is designed to have good imaging properties, then middle and high spatial frequency errors in the test system can be well calibrated. The improved imaging properties are provided by a rudimentary auxiliary optic as part of the calibration system. The

auxiliary optic is simple to characterize and align to the CGH. Use of the auxiliary optic also reduces the size of the CGH required for calibration and the density of the lines required for the CGH. The resulting CGH is less expensive than the existing technology and has reduced write error and alignment error sensitivities.

This CGH system is suitable for any kind of calibration using an interferom-

eter when high spatial resolution is required. It is especially well suited for tests that include segmented optical components or large apertures.

This work was done by Gene Olczak of ITT Geospatial Systems for Goddard Space Flight Center. For further information, contact the Goddard Innovative Partnerships Office at (301) 286-5810. GSC-15676-1

Non-Contact Thermal Properties Measurement With Low-Power Laser and IR Camera System

Photons both excite and are used to measure the thermal response of any surface material.

NASA's Jet Propulsion Laboratory, Pasadena, California

As shown by the Phoenix Mars Lander's Thermal and Electrical Conductivity Probe (TECP), contact measurements of thermal conductivity and diffusivity (using a modified flux-plate or line-source heat-pulse method) are constrained by a number of factors. Robotic resources must be used to place the probe, making them unavailable for other operations for the duration of the measurement. The range of placement is also limited by mobility, particularly in the case of a lander. Placement is also subject to irregularities in contact quality, resulting in non-repeatable heat transfer to the material under test. Most important from a scientific perspective, the varieties of materials which can be measured are limited to unconsolidated or weakly-cohesive regolith materials, rocks, and ices being too hard for nominal insertion strengths.

Accurately measuring thermal properties in the laboratory requires significant experimental finesse, involving sample preparation, controlled and repeatable procedures, and, practically, instrumentation much more voluminous than the sample being tested (heater plates, insulation, temperature sensors). Remote measurements (infrared images from orbiting spacecraft) can reveal composite properties

like thermal inertia, but suffer both from a large footprint (low spatial resolution) and convolution of the thermal properties of a potentially layered medium. *In situ* measurement techniques (the Phoenix TECP is the only robotic measurement of thermal properties to date) suffer from problems of placement range, placement quality, occupation of robotic resources, and the ability to only measure materials of low mechanical strength.

A spacecraft needs the ability to perform a non-contact thermal properties measurement *in situ*. Essential components include low power consumption, leveraging of existing or highly-developed flight technologies, and mechanical simplicity.

This new *in situ* method, by virtue of its being non-contact, bypasses all of these problems. The use of photons to both excite and measure the thermal response of any surface material to a high resolution (estimated footprint $\approx 10 \text{ cm}^2$) is a generational leap in physical properties measurements.

The proposed method consists of spot-heating the surface of a material with a low ($<1 \text{ W}$) power laser. This produces a moderate (5-10 K) temperature increase in the material. As the heat propagates in a hemisphere from the point of heating, it raises the tempera-

ture of the surrounding surface. The temperature of the heating spot itself, and that of the surrounding material, is monitored remotely with an infrared camera system. Monitoring is done during both the heating and cooling (after the laser is turned off) phases. Temperature evolution as a function of distance from the heating point contains information about the material's thermal properties, and can be extracted through curve-fitting to analytical models of heat transport.

In situ measurement of thermal properties of planetary surface materials provides ground-truth for remote sensing observations and high-resolution, site-specific data for any landed spacecraft environment. Thermal properties are necessary parameters for modeling and understanding thermal evolution of the surface and subsurface, climate state and history, and predicting the presence of subsurface water/ice. The applications extend to all solid bodies in the solar system, but with greatest applicability to bodies with thin or tenuous atmospheres where conduction and radiation are the dominant heat-transport properties.

This work was done by Troy L. Hudson and Michael H. Hecht of Caltech for NASA's Jet Propulsion Laboratory. Further information is contained in a TSP (see page 1). NPO-47390



SpaceCube 2.0: An Advanced Hybrid Onboard Data Processor

Two FPGAs maximize data and computing performance while minimizing physical size.

Goddard Space Flight Center, Greenbelt, Maryland

The SpaceCube 2.0 is a compact, high-performance, low-power onboard processing system that takes advantage of cutting-edge hybrid (CPU/FPGA/DSP) processing elements. The SpaceCube 2.0 design concept includes two commercial Virtex-5 field-programmable gate array (FPGA) parts protected by “radiation hardened by software” technology, and possesses exceptional size, weight, and power characteristics [5×5×7 in., 3.5 lb (=12.7×12.7×17.8 cm, 1.6 kg) 5–25 W, depending on the application’s required clock rate]. The two Virtex-5 FPGA parts are implemented in a unique back-to-back configuration to maximize data transfer and computing performance.

Draft computing power specifications for the SpaceCube 2.0 unit include four

PowerPC 440s (1100 DMIPS each), 500+ DSP48Es (2×580 GMACS), 100+ LVDS high-speed serial I/Os (1.25 Gbps each), and 2×190 GFLOPS single-precision (65 GFLOPS double-precision) floating point performance. The SpaceCube 2.0 includes PROM memory for CPU boot, health and safety, and basic command and telemetry functionality; RAM memory for program execution; and FLASH/EEPROM memory to store algorithms and application code for the CPU, FPGA, and DSP processing elements. Program execution can be reconfigured in real time and algorithms can be updated, modified, and/or replaced at any point during the mission. Gigabit Ethernet, Spacewire, SATA and high-speed LVDS serial/parallel I/O chan-

nels are available for instrument/sensor data ingest, and mission-unique instrument interfaces can be accommodated using a compact PCI (cPCI) expansion card interface.

The SpaceCube 2.0 can be utilized in NASA Earth Science, Helio/Astro-physics and Exploration missions, and Department of Defense satellites for onboard data processing. It can also be used in commercial communication and mapping satellites.

This work was done by Michael Lin, Thomas Flatley, John Godfrey, Alessandro Geist, Daniel Espinosa, and David Petrick of Goddard Space Flight Center. Further information is contained in a TSP (see page 1). GSC-15760-1

CMOS Imager Has Better Cross-Talk and Full-Well Performance

Electrically isolated areas containing imaging and readout structures are optimized separately.

NASA’s Jet Propulsion Laboratory, Pasadena, California

A complementary metal oxide/semiconductor (CMOS) image detector now undergoing development is designed to exhibit less cross-talk and greater full-well capacity than do prior CMOS image detectors of the same type. Imagers of the type in question are designed to operate from low-voltage power supplies and are fabricated by processes that yield device features having dimensions in the deep submicron range.

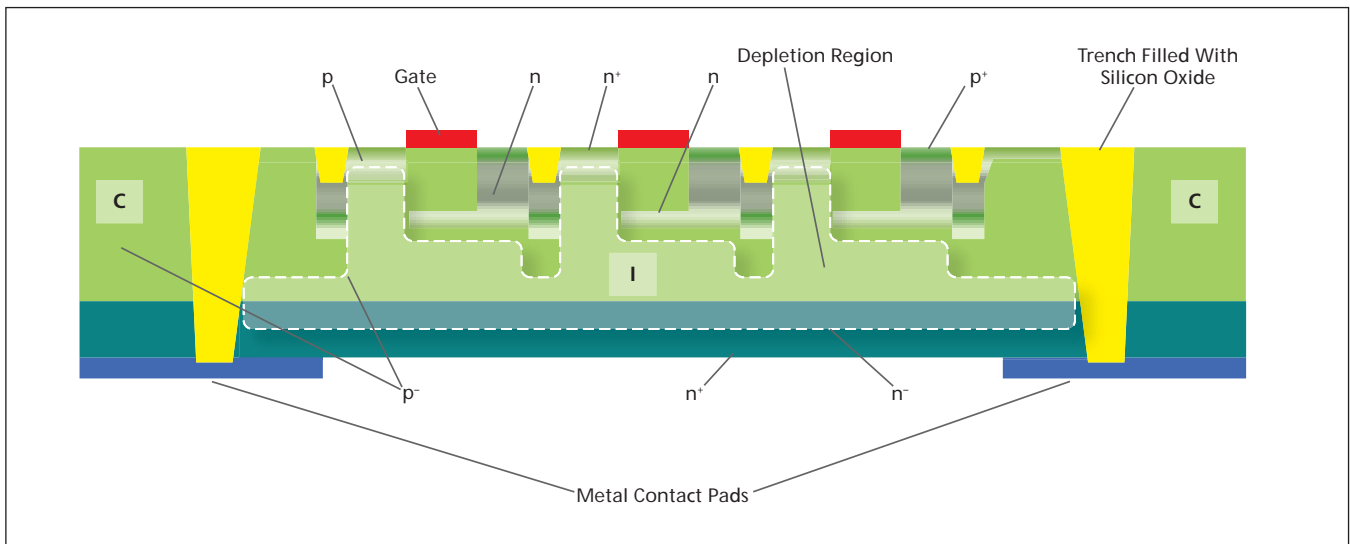
Because of the use of low supply potentials, maximum internal electric fields and depletion widths are correspondingly limited. In turn, these limitations are responsible for increases in cross-talk and decreases in charge-handling capacities. Moreover, for small pixels, lateral depletion cannot be extended. These adverse effects are even more accentuated in a back-illuminated CMOS imager, in which photogenerated charge carriers must travel across the entire thickness of the device.

The figure shows a partial cross section of the structure in the device layer of the present developmental CMOS imager. (In a practical imager, the device layer would sit atop either a heavily doped silicon substrate or a thin silicon oxide layer on a silicon substrate, not shown here.) The imager chip is divided into two areas: area C, which contains readout circuits and other electronic circuits; and area I, which contains the imaging (photodetector and photogenerated-charge-collecting) pixel structures. Areas C and I are electrically isolated from each other by means of a trench filled with silicon oxide.

The electrical isolation between areas C and I makes it possible to apply different supply potentials to these areas, thereby enabling optimization of the supply potential and associated design features for each area. More specifically, metal oxide semiconductor field-effect transistors (MOSFETs) that are typically included in CMOS imagers

now reside in area C and can remain unchanged from established designs and operated at supply potentials prescribed for those designs, while the dopings and the lower supply potentials in area I can be tailored to optimize imager performance.

In area I, the device layer includes an n⁺-doped silicon layer on which is grown an n⁻-doped silicon layer. A p⁻-doped silicon layer is grown on top of the n⁻-doped layer. The total imaging device thickness is the sum of the thickness of the n⁺, n, and p⁻ layers. A pixel photodiode is formed between a surface n⁺ implant, a p implant underneath it, the aforementioned p⁻ layer, and the n⁻ and n⁺ layers. Adjacent to the diode is a gate for transferring photogenerated charges out of the photodiode and into a floating diffusion formed by an implanted p⁺ layer on an implanted n-doped region. Metal contact pads are added to the back-side for providing back-side bias.



This **Simplified Cross Section** (not to scale) shows essential features of the developmental device structure. A key feature of the structure is the depletion region (indicated by the dashed outline) along the entire n⁻/p⁻ junction.

The n⁻ and p⁻ doping concentrations are chosen such that everywhere in area I, a depletion region exists between the n⁻ and p⁻ layers. This depletion region enables electrical isolation between the several front (top) doped regions and the back (bottom) n and n⁺ layers. Consequently, the bias potentials applied to the top of the diode and the adjacent transfer gate can be different from the bias applied to the bottom. Thus, while CMOS-compatible potentials (e.g., 3 V) are applied at the top, the bottom of the structure can be biased to greater potential (e.g., 5 V) via the back-side metal contact pads to completely deplete the photodiode. The re-

sulting depletion region is indicated in the figure as the area enclosed by the dashed outline. Complete depletion of the photodiode results in collection of charge carriers (holes in this case) under the influence of an electric field, and hence, a significant reduction of cross-talk. Complete depletion also increases the charge-storage volume, and, hence, the charge-handling capacity. Thus, the structure described here provides for large depletion width around each photodiode, independent of the CMOS power-supply voltage and pixel size.

This work was done by Bedabrata Pain and Thomas J. Cunningham of Caltech for NASA's

Jet Propulsion Laboratory. Further information is contained in a TSP (see page 1).

In accordance with Public Law 96-517, the contractor has elected to retain title to this invention. Inquiries concerning rights for its commercial use should be addressed to:

*Innovative Technology Assets Management
JPL*

Mail Stop 202-233

4800 Oak Grove Drive

Pasadena, CA 91109-8099

E-mail: iaoffice@jpl.nasa.gov

Refer to NPO-45964, volume and number of this NASA Tech Briefs issue, and the page number.

High-Performance Wireless Telemetry

This technology is applicable to any kind of aviation or power-plant turbine testing.

John H. Glenn Research Center, Cleveland, Ohio

Prior technology for machinery data acquisition used slip rings, FM radio communication, or non-real-time digital communication. Slip rings are often noisy, require much space that may not be available, and require access to the shaft, which may not be possible. FM radio is not accurate or stable, and is limited in the number of channels, often with channel crosstalk, and intermittent as the shaft rotates. Non-real-time digital communication is very popular, but complex, with long development time, and objections from users who need continuous waveforms from many channels.

This innovation extends the amount of information conveyed from a rotating machine to a data acquisition system

while keeping the development time short and keeping the rotating electronics simple, compact, stable, and rugged. The data are all real time. The product of the number of channels, times the bit resolution, times the update rate, gives a data rate higher than available by older methods. The telemetry system consists of a data-receiving rack that supplies magnetically coupled power to a rotating instrument amplifier ring in the machine being monitored. The ring digitizes the data and magnetically couples the data back to the rack, where it is made available.

The transformer is generally a ring positioned around the axis of rotation with one side of the transformer free to

rotate and the other side held stationary. The windings are laid in the ring; this gives the data immunity to any rotation that may occur.

A medium-frequency sine-wave power source in a rack supplies power through a cable to a rotating ring transformer that passes the power on to a rotating set of electronics. The electronics power a set of up to 40 sensors and provides instrument amplifiers for the sensors. The outputs from the amplifiers are filtered and multiplexed into a serial ADC. The output from the ADC is connected to another rotating ring transformer that conveys the serial data from the rotating section to the stationary section. From there, a cable conveys the serial data to

the remote rack, where it is reconditioned to logic level specifications, deserialized, and converted back to analog. In the rotating electronics are code generators to indicate the beginning of files for data synchronization.

An alternative method would be to use two symmetrical coils. Since the two coils are rotationally symmetrical, rotation does not influence the magnetic coupling from the primary to the secondary. Since the secondary coil is electrostatically shielded, environmental noise pickup is intrinsically low. Since the transformer is air-core, the uncompressed bandwidth can be high — 50 MHz, 200 MHz, or higher.

The rotating coil is the primary component of the transformer and is in the

shape of a thin ring, containing a few turns of wire. The plane of the ring is perpendicular to the axis of rotation. Radially, just beyond the rotating primary coil, is the secondary coil in the shape of a ring, and lying close to the primary. The secondary coil is a single turn of coaxial cable with the center conductor connected to the shield of the cable where it leaves the coil. The binary data are fed into both ends of the primary coil through an impedance matching resistor, with one end receiving the data inverted. This double-ended (full-bridge) approach reduces propagation delay distortions and increases signal strength. The secondary coil has an impedance matching resistor at the end of the cable. Use of a coaxial cable reduces ca-

pacitive coupling, but freely allows magnetic coupling. To enhance the coupling, ferrite cloth can be laid into a groove and the primary coil wound on top of it. Similarly, ferrite cloth can be formed around the secondary coil. Copper rings can be placed on either side of the coil set to reduce outside influences.

This work was done by Elmer Griebeler, Nuha Nawash, and James Buckley of Glenn Research Center. Further information is contained in a TSP (see page 1).

Inquiries concerning rights for the commercial use of this invention should be addressed to NASA Glenn Research Center, Innovative Partnerships Office, Attn: Steven Fedor, Mail Stop 4-8, 21000 Brookpark Road, Cleveland, Ohio 44135. Refer to LEW-18575-1/7-1.

Telemetry-Based Ranging

NASA's Jet Propulsion Laboratory, Pasadena, California

A telemetry-based ranging scheme was developed in which the downlink ranging signal is eliminated, and the range is computed directly from the downlink telemetry signal. This is the first Deep Space Network (DSN) ranging technology that does not require the spacecraft to transmit a separate ranging signal. By contrast, the evolutionary ranging techniques used over the years by NASA missions, including sequential ranging (transmission of a sequence of sinusoids) and PN-ranging (transmission of a pseudo-noise sequence) — whether regenerative (spacecraft acquires, then regenerates and retransmits a noise-free ranging signal) or transparent (spacecraft feeds the noisy demodulated uplink ranging

signal into the downlink phase modulator) — relied on spacecraft power and bandwidth to transmit an explicit ranging signal.

The state of the art in ranging is described in an emerging CCSDS (Consultative Committee for Space Data Systems) standard, in which a pseudo-noise (PN) sequence is transmitted from the ground to the spacecraft, acquired onboard, and the PN sequence is coherently retransmitted back to the ground, where a delay measurement is made between the uplink and downlink signals. In this work, the telemetry signal is aligned with the uplink PN code epoch. The ground station computes the delay between the uplink signal transmission and the re-

ceived downlink telemetry. Such a computation is feasible because symbol synchronizability is already an integral part of the telemetry design.

Under existing technology, the telemetry signal cannot be used for ranging because its arrival-time information is not coherent with any Earth reference signal. By introducing this coherence, and performing joint telemetry detection and arrival-time estimation on the ground, a high-rate telemetry signal can provide all the precision necessary for spacecraft ranging.

This work was done by Jon Hamkins, Victor A. Vilnrotter, Kenneth S. Andrews, and Shervin Shambayati of Caltech for NASA's Jet Propulsion Laboratory. For more information, contact iaoffice@jpl.nasa.gov. NPO-47170



JWST Wavefront Control Toolbox

A Matlab-based toolbox has been developed for the wavefront control and optimization of segmented optical surfaces to correct for possible misalignments of James Webb Space Telescope (JWST) using influence functions. The toolbox employs both iterative and non-iterative methods to converge to an optimal solution by minimizing the cost function. The toolbox could be used in either of constrained and unconstrained optimizations. The control process involves 1 to 7 degrees-of-freedom perturbations per segment of primary mirror in addition to the 5 degrees of freedom of secondary mirror.

The toolbox consists of a series of Matlab/Simulink functions and modules, developed based on a “wrapper” approach, that handles the interface and data flow between existing commercial optical modeling software packages such as Zemax and Code V. The limitations of the algorithm are dictated by the constraints of the moving parts in the mirrors.

This work was done by Shahram Ron Shiri and David L. Aronstein of Goddard Space Flight Center. For further information, contact the Goddard Innovative Partnerships Office (301) 286-5810. GSC-15567-1

Java Image I/O for VICAR, PDS, and ISIS

This library, written in Java, supports input and output of images and metadata (labels) in the VICAR, PDS image, and ISIS-2 and ISIS-3 file formats. Three levels of access exist.

The first level comprises the low-level, direct access to the file. This allows an application to read and write specific image tiles, lines, or pixels and to manipulate the label data directly. This layer is analogous to the C-language “VICAR Run-Time Library” (RTL), which is the image I/O library for the (C/C++/Fortran) VICAR image processing system from JPL MIPL (Multi-mission Image Processing Lab). This low-level library can also be used to read

and write labeled, uncompressed images stored in formats similar to VICAR, such as ISIS-2 and -3, and a subset of PDS (image format).

The second level of access involves two codecs based on Java Advanced Imaging (JAI) to provide access to VICAR and PDS images in a file-format-independent manner. JAI is supplied by Sun Microsystems as an extension to desktop Java, and has a number of codecs for formats such as GIF, TIFF, JPEG, etc. Although Sun has deprecated the codec mechanism (replaced by IIO), it is still used in many places. The VICAR and PDS codecs allow any program written using the JAI codec spec to use VICAR or PDS images automatically, with no specific knowledge of the VICAR or PDS formats. Support for metadata (labels) is included, but is format-dependent. The PDS codec, when processing PDS images with an embedded VIAR label (“dual-labeled images,” such as used for MER), presents the VICAR label in a new way that is compatible with the VICAR codec.

The third level of access involves VICAR, PDS, and ISIS Image I/O plugins. The Java core includes an “Image I/O” (IIO) package that is similar in concept to the JAI codec, but is newer and more capable. Applications written to the IIO specification can use any image format for which a plug-in exists, with no specific knowledge of the format itself.

This work was done by Robert G. Deen and Steven R. Levee of Caltech for NASA’s Jet Propulsion Laboratory. For more information, contact iaoffice@jpl.nasa.gov.

This software is available for commercial licensing. Please contact Daniel Broderick of the California Institute of Technology at danielb@caltech.edu. Refer to NPO-47184.

X-Band Acquisition Aid Software

The X-band Acquisition Aid (AAP) software is a low-cost acquisition aid for the Deep Space Network (DSN) antennas, and is used while acquiring a spacecraft shortly after it has launched. When enabled, the acquisition aid provides

corrections to the antenna-predicted trajectory of the spacecraft to compensate for the variations that occur during the actual launch. The AAP software also provides the corrections to the antenna-predicted trajectory to the navigation team that uses the corrections to refine their model of the spacecraft in order to produce improved antenna-predicted trajectories for each spacecraft that passes over each complex.

The software provides an automated Acquisition Aid receiver calibration, and provides graphical displays to the operator and remote viewers via an Ethernet connection. It has a Web server, and the remote workstations use the Firefox browser to view the displays. At any given time, only one operator can control any particular display in order to avoid conflicting commands from more than one control point. The configuration and control is accomplished solely via the graphical displays. The operator does not have to remember any commands. Only a few configuration parameters need to be changed, and can be saved to the appropriate spacecraft-dependent configuration file on the AAP’s hard disk.

AAP automates the calibration sequence by first commanding the antenna to the correct position, starting the receiver calibration sequence, and then providing the operator with the option of accepting or rejecting the new calibration parameters. If accepted, the new parameters are stored in the appropriate spacecraft-dependent configuration file. The calibration can be performed on the Sun, greatly expanding the window of opportunity for calibration. The spacecraft traditionally used for calibration is in view typically twice per day, and only for about ten minutes each pass.

This work was done by Michael J. Britcliffe and Martha M. Strain of Caltech and Michael Wert of ITT for NASA’s Jet Propulsion Laboratory. Further information is contained in a TSP (see page 1).

The software used in this innovation is available for commercial licensing. Please contact Daniel Broderick of the California Institute of Technology at danielb@caltech.edu. Refer to NPO-47004.



Antimicrobial-Coated Granules for Disinfecting Water

Lyndon B. Johnson Space Center, Houston, Texas

Methods of preparing antimicrobial-coated granules for disinfecting flowing potable water have been developed. Like the methods reported in the immediately preceding article, these methods involve chemical preparation of substrate surfaces (in this case, the surfaces of granules) to enable attachment of antimicrobial molecules to the surfaces via covalent bonds. A variety of granular materials have been coated with a vari-

ety of antimicrobial agents that include antibiotics, bacteriocins, enzymes, bactericides, and fungicides. When employed in packed beds in flowing water, these antimicrobial-coated granules have been proven effective against gram-positive bacteria, gram-negative bacteria, fungi, and viruses. Composite beds, consisting of multiple layers containing different granular antimicrobial media, have proven particularly effec-

tive against a broad spectrum of microorganisms. These media have also proven effective in enhancing or potentiating the biocidal effects of in-line iodinated resins and of very low levels of dissolved elemental iodine.

This work was done by James R. Akse, John T. Holtsnider, and Helen Kliestik of Umpqua Research Co. for Johnson Space Center. Further information is contained in a TSP (see page 1). MSC-23468-1

Range 7 Scanner Integration With PaR Robot Scanning System

Models of complex objects can be developed even if the objects are large and featureless.

John F. Kennedy Space Center, Florida

An interface bracket and coordinate transformation matrices were designed to allow the Range 7 scanner to be mounted on the PaR Robot detector arm for scanning the heat shield or other object placed in the test cell. A process was designed for using Rapid Form XOR to stitch data from multiple scans together to provide an accurate 3D model of the object scanned.

An accurate model was required for the design and verification of an existing heat shield. The large physical size and complex shape of the heat shield does not allow for direct measurement of certain features in relation to other features. Any imaging devices capable of imaging the entire heat shield in its entirety suffers a reduced resolution and cannot image sections that are blocked from view. Prior methods involved tools such as commercial measurement arms, tak-

ing images with cameras, then performing manual measurements. These prior methods were tedious and could not provide a 3D model of the object being scanned, and were typically limited to a few tens of measurement points at prominent locations.

Integration of the scanner with the robot allows for large complex objects to be scanned at high resolution, and for 3D Computer Aided Design (CAD) models to be generated for verification of items to the original design, and to generate models of previously undocumented items.

The main components are the mounting bracket for the scanner to the robot and the coordinate transformation matrices used for stitching the scanner data into a 3D model. The steps involve mounting the interface bracket to the robot's detector arm, mounting the scan-

ner to the bracket, and then scanning sections of the object and recording the location of the tool tip (in this case the center of the scanner's focal point).

A novel feature is the ability to stitch images together by coordinates instead of requiring each scan data set to have overlapping identifiable features. This setup allows models of complex objects to be developed even if the object is large and featureless, or has sections that don't have visibility to other parts of the object for use as a reference. In addition, millions of points can be used for creation of an accurate model [i.e. within 0.03 in. (≈ 0.8 mm) over a span of 250 in. (≈ 635 mm)].

This work was done by Bradley Burns, Jeffrey Carlson, Mark Minich, and Jason Schuler of Kennedy Space Center. Further information is contained in a TSP (see page 1). KSC-13489/95

Methods of Antimicrobial Coating of Diverse Materials

Lyndon B. Johnson Space Center, Houston, Texas

Methods of coating diverse substrate materials with antimicrobial agents have been developed. Originally intended to reduce health risks to astronauts posed by pathogenic microorgan-

isms that can grow on surfaces in spacecraft, these methods could also be used on Earth — for example, to ensure sterility of surgical inserts and other medical equipment. The methods in-

volve, generally, chemical preparation of substrate surfaces to enable attachment of antimicrobial molecules to the substrate surfaces via covalent bonds. Substrate materials that have been

treated successfully include aluminum, glass, a corrosion-resistant nickel alloy, stainless steel, titanium, and poly(tetrafluoroethylene). Antimicrobial agents that have been successfully immobilized include antibiotics, enzymes, bacteriocins, bactericides, and fungicides.

A variety of linkage chemistries were employed. Activity of antimicrobial coatings against gram-positive bacteria, gram-negative bacteria, and fungi was demonstrated. Results of investigations indicate that the most suitable combination of antimicrobial agent, sub-

strate, and coating method depends upon the intended application.

This work was done by James R. Akse, John T. Holtsnider, and Helen Kliestik of Umpqua Research Co. for Johnson Space Center. For further information, contact the Johnson Commercial Technology Office at (281) 483-3809. MSC-23467-1

High-Operating-Temperature Barrier Infrared Detector With Tailorable Cutoff Wavelength

Novel materials allow the detector to operate at higher temperatures.

NASA's Jet Propulsion Laboratory, Pasadena, California

A mid-wavelength infrared (MWIR) barrier photodetector is capable of operating at higher temperature than the prevailing MWIR detectors based on InSb. The standard high-operating-temperature barrier infrared detector (HOT-BIRD) is made with an InAsSb infrared absorber that is lattice-matched to a GaSb substrate, and has a cutoff wavelength of approximately 4 microns. To increase the versatility and utility of the HOT-BIRD, it is implemented with IR absorber materials with customizable cutoff wavelengths.

The HOT-BIRD can be built with the quaternary alloy GaInAsSb as the absorber, GaAlSbAs as the barrier, on a lattice-matching GaSb substrate. The cutoff wavelength of the GaInAsSb can be tailored by adjusting the alloy composition. To build a HOT-BIRD requires a matching pair of absorber and barrier materials with the following properties: (1) their valence band edges must be approximately the same to allow unimpeded hole flow, while their conduction

band edges should have a large difference to form an electron barrier; and (2) the absorber and the barrier must be respectively lattice-matched and closely lattice-matched to the substrate to ensure high material quality and low defect density.

To make a HOT-BIRD with cutoff wavelength shorter than 4 microns, a GaInAsSb quaternary alloy was used as the absorber, and a matching GaAlSbAs quaternary alloy as the barrier. By changing the alloy composition, the band gap of the quaternary alloy absorber can be continuously adjusted with cutoff wavelength ranging from 4 microns down to the short wavelength infrared (SWIR). By carefully choosing the alloy composition of the barrier, a HOT-BIRD structure can be formed. With this method, a HOT-BIRD can be made with continuously tailorable cutoff wavelengths from 4 microns down to the SWIR.

The HOT-BIRD detector technology is suitable for making very-large-format

MWIR/SWIR focal plane arrays that can be operated by passive cooling from low Earth orbit. High-operating-temperature infrared with reduced cooling requirement would benefit space missions in reduction of size, weight, and power, and an increase in mission lifetime.

This work was done by David Z. Ting, Cory J. Hill, Alexander Soibel, Sumith V. Bandara, and Sarath D. Gunapala of Caltech for NASA's Jet Propulsion Laboratory. For more information, contact iaoffice@jpl.nasa.gov.

In accordance with Public Law 96-517, the contractor has elected to retain title to this invention. Inquiries concerning rights for its commercial use should be addressed to:

*Innovative Technology Assets Management
JPL*

Mail Stop 202-233

4800 Oak Grove Drive

Pasadena, CA 91109-8099

E-mail: iaoffice@jpl.nasa.gov

Refer to NPO-46477, volume and number of this NASA Tech Briefs issue, and the page number.



A Model of Reduced Kinetics for Alkane Oxidation Using Constituents and Species for N-Heptane

When certain variables are judiciously combined, a self-similarity appears, allowing for a compact chemistry reduction mechanism that predicts ignition time.

NASA's Jet Propulsion Laboratory, Pasadena, California

The reduction of elementary or skeletal oxidation kinetics to a subgroup of tractable reactions for inclusion in turbulent combustion codes has been the subject of numerous studies. The skeletal mechanism is obtained from the elementary mechanism by removing from it reactions that are considered negligible for the intent of the specific study considered. As of now, there are many chemical reduction methodologies.

A methodology for deriving a reduced kinetic mechanism for alkane oxidation is described and applied to n-heptane. The model is based on partitioning the species of the skeletal kinetic mechanism into lights, defined as those having a carbon number smaller than 3, and heavies, which are the complement of the species ensemble. For modeling purposes, the heavy species are mathematically decomposed into constituents, which are similar but not identical to groups in the group additivity theory.

From analysis of the LLNL (Lawrence Livermore National Laboratory) skeletal mechanism in conjunction with CHEMKIN II, it is shown that a similarity variable can be formed such that the appropriately non-dimensionalized

global constituent molar density exhibits a self-similar behavior over a very wide range of equivalence ratios, initial pressures and initial temperatures that is of interest for predicting n-heptane oxidation. Furthermore, the oxygen and water molar densities are shown to display a quasi-linear behavior with respect to the similarity variable. The light species ensemble is partitioned into quasi-steady and unsteady species. The reduced model is based on concepts consistent with those of Large Eddy Simulation (LES) in which functional forms are used to replace the small scales eliminated through filtering of the governing equations; in LES, these small scales are unimportant as far as the overwhelming part of dynamic energy is concerned.

Here, the scales thought unimportant for recovering the thermodynamic energy are removed. The concept is tested by using tabular information from the LLNL skeletal mechanism in conjunction with CHEMKIN II utilized as surrogate ideal functions replacing the necessary functional forms. The test reveals that the similarity concept is indeed justified and that the combustion tempera-

ture is well predicted, but that the ignition time is over-predicted, a fact traced to neglecting a detailed description of the processes leading to the heavies chemical decomposition. To palliate this deficiency, functional modeling is incorporated into this conceptual reduction in addition to the modeling the evolution of the global constituent molar density, the enthalpy evolution of the heavies, the contribution to the reaction rate of the unsteady lights from other light species and from the heavies, the molar density evolution of oxygen and water, and the mole fractions of the quasi-steady light species.

The model is compact in that there are only nine species-related progress variables. Results are presented showing the performance of the model for predicting the temperature and species evolution. The model reproduces the ignition time over a wide range of equivalence ratios, initial pressure, and initial temperature.

This work was done by Kenneth G. Harstad and Josette Bellan of Caltech for NASA's Jet Propulsion Laboratory. For more information, contact iaoffice@jpl.nasa.gov. NPO-47383

Thermally Conductive Tape Based on Carbon Nanotube Arrays

This material can be used for thermal management of microelectronic packages and electronic systems.

Goddard Space Flight Center, Greenbelt, Maryland

To increase contact conductance between two mating surfaces, a conductive "tape" has been developed by growing dense arrays of carbon nanotubes (CNTs, graphite layers folded into cylinders) on both sides of a thermally conductive metallic foil. When the two mating surfaces are brought into contact with the conductive tape in between, the CNT arrays will adhere to the mating surface.

The van der Waals force between the contacting tubes and the mating surface provides adhesion between the two mating surfaces. Even though the thermal contact conductance of a single tube-to-tube contact is small, the tremendous amount of CNTs on the surface leads to a very large overall contact conductance.

Interface contact thermal resistance rises from the microroughness and the macro-

scopic non-planar quality of mating surfaces. When two surfaces come into contact with each other, the actual contact area may be much less than the total area of the surfaces. The real area of contact depends on the load, the surface roughness, and the elastic and inelastic properties of the surface. This issue is even more important at cryogenic temperatures, where materials become hard and brittle and vacuum is

used, which prevents any gas conduction through the interstitial region.

A typical approach to increase thermal contact conductance is to use thermally conducting epoxies or greases, which are not always compatible with vacuum conditions. In addition, the thermal conductivities of these compounds are often relatively low. The CNTs used in this approach can be metallic or semiconducting, depending on the folding angle and diameter. The electrical resistivity of multiwalled carbon nanotubes (MWCNTs) has been reported. MWCNTs can pass a

current density and remain stable at high temperatures in air. The thermal conductivity of a MWCNT at room temperature is measured to be approximately 3,000 W/m-K, which is much larger than that of diamond. At room temperature, the thermal conductance of a 0.3 cm² array of CNTs was measured to be as high as 10 W/K. The high thermal conductivity and the nanoscale size make CNTs ideal as thermal interface materials.

The CNT-based thermal tape can be used for the thermal management of microelectronic packages and electronic

systems. It also can be integrated with current device technology and packaging. The material would allow for an efficient method to manage excess heat generation without requiring any additional power. Lastly, the CNT tape can be used to enhance thermal contact conductance across two mating surfaces on some NASA missions.

This work was done by Ali Kashani of Atlas Scientific for Goddard Space Flight Center. For further information, contact the Goddard Innovative Partnerships Office at (301) 286-5810. GSC-15607-1

Two Catalysts for Selective Oxidation of Contaminant Gases

One oxidizes halocarbons and ammonia; the other oxidizes ammonia.

Lyndon B. Johnson Space Center, Houston, Texas

Two catalysts for the selective oxidation of trace amounts of contaminant gases in air have been developed for use aboard the International Space Station. These catalysts might also be useful for reducing concentrations of fumes in terrestrial industrial facilities — especially facilities that use halocarbons as solvents, refrigerant liquids, and foaming agents, as well as facilities that generate or utilize ammonia.

The first catalyst is of the supported-precious-metal type. This catalyst is highly active for the oxidation of halocarbons, hydrocarbons, and oxygenates at low concentrations in air. This catalyst is more active for the oxidation of hydrocarbons and halocarbons than are competing catalysts developed in recent years. This catalyst completely converts these airborne contaminant gases to carbon dioxide, water, and mineral acids that can be easily re-

moved from the air, and does not make any chlorine gas in the process. The catalyst is thermally stable and is not poisoned by chlorine or fluorine atoms produced on its surface during the destruction of a halocarbon. In addition, the catalyst can selectively oxidize ammonia to nitrogen at a temperature between 200 and 260 °C, without making nitrogen oxides, which are toxic. The temperature of 260 °C is higher than the operational temperature of any other precious-metal catalyst that can selectively oxidize ammonia.

The purpose of the platinum in this catalyst is to oxidize hydrocarbons and to ensure that the oxidation of halocarbons goes to completion. However, the platinum exhibits little or no activity for initiating the destruction of halocarbons. Instead, the attack on the halocarbons is initiated by the support. The support also provides a high sur-

face area for exposure of the platinum. Moreover, the support resists deactivation or destruction by halogens released during the destruction of halocarbons.

The second catalyst is of the supported-metal-oxide type. This catalyst can selectively oxidize ammonia to nitrogen at temperatures up to 400 °C, without producing nitrogen oxides. This catalyst converts ammonia completely to nitrogen, even when the concentration of ammonia is very low. No other catalyst is known to oxidize ammonia selectively at such a high temperature and low concentration. Both the metal oxide and the support contribute to the activity and selectivity of this catalyst.

This work was done by John D. Wright of TDA Research for Johnson Space Center. For further information, contact the JSC Innovation Partnerships Office at (281) 483-3809. MSC-23054-1

Nanoscale Metal Oxide Semiconductors for Gas Sensing

John H. Glenn Research Center, Cleveland, Ohio

A report describes the fabrication and testing of nanoscale metal oxide semiconductors (MOSs) for gas and chemical sensing. This document examines the relationship between processing approaches and resulting sensor behavior. This is a core question related to a range of applications of nanotechnology and a number of different synthesis methods are discussed: thermal evapo-

ration-condensation (TEC), controlled oxidation, and electrospinning. Advantages and limitations of each technique are listed, providing a processing overview to developers of nanotechnology-based systems.

The results of a significant amount of testing and comparison are also described. A comparison is made between SnO₂, ZnO, and TiO₂ single-crystal

nanowires and SnO₂ polycrystalline nanofibers for gas sensing. The TEC-synthesized single-crystal nanowires offer uniform crystal surfaces, resistance to sintering, and their synthesis may be done apart from the substrate. The TEC-produced nanowire response is very low, even at the operating temperature of 200 °C. In contrast, the electrospun polycrystalline nanofiber response is

high, suggesting that junction potentials are superior to a continuous surface depletion layer as a transduction mechanism for chemisorption. Using a catalyst deposited upon the surface in the form of nanoparticles yields dramatic gains in sensitivity for both nanostructured, one-dimensional forms.

For the nanowire materials, the response magnitude and response rate uniformly increase with increasing operating temperature. Such changes are interpreted in terms of accelerated surface diffusional processes, yielding

greater access to chemisorbed oxygen species and faster dissociative chemisorption, respectively. Regardless of operating temperature, sensitivity of the nanofibers is a factor of 10 to 100 greater than that of nanowires with the same catalyst for the same test condition. In summary, nanostructure appears critical to governing the reactivity, as measured by electrical resistance of these SnO₂ nanomaterials towards reducing gases. With regard to the sensitivity of the different nascent nanostructures, the electrospon nanofibers appear preferable.

This work was done by Gary W. Hunter, Laura Evans, and Jennifer C. Xu of Glenn Research Center; Randy L. Vander Wal of Penn State University; and Gordon M. Berger and Michael J. Kulis of the National Center for Space Exploration Research. Further information is contained in a TSP (see page 1).

Inquiries concerning rights for the commercial use of this invention should be addressed to NASA Glenn Research Center, Innovative Partnerships Office, Attn: Steven Fedor, Mail Stop 4-8, 21000 Brookpark Road, Cleveland, Ohio 44135. Refer to LEW-18492-1.

Lightweight, Ultra-High-Temperature, CMC-Lined Carbon/Carbon Structures

This refractory composite material is applicable to defense vehicles, combustion chambers, rocket nozzles, hot gas generators, and valves using both liquid and solid propellants.

John H. Glenn Research Center, Cleveland, Ohio

Carbon/carbon (C/C) is an established engineering material used extensively in aerospace. The beneficial properties of C/C include high strength, low density, and toughness. Its shortcoming is its limited usability at temperatures higher than the oxidation temperature of carbon — approximately 400 °C. Ceramic matrix composites (CMCs) are used instead, but carry a weight penalty. Combining a thin laminate of CMC to a bulk structure of C/C retains all of the benefits of C/C with the high temperature oxidizing environment usability of CMCs.

Ultramet demonstrated the feasibility of combining the light weight of C/C composites with the oxidation resistance of zirconium carbide (ZrC) and zirconium-silicon carbide (Zr-Si-C) CMCs in a unique system composed of a C/C primary structure with an integral CMC liner with temperature capability up to 4,200 °F (≈2,315 °C). The system effectively bridged the gap in weight and performance between coated C/C and bulk CMCs. Fabrication was demonstrated through an innovative variant of Ultra-

met's rapid, pressureless melt infiltration processing technology. The fully developed material system has strength that is comparable with that of C/C, lower density than Cf/SiC, and ultra-high-temperature oxidation stability. Application of the reinforced ceramic casing to a predominantly C/C structure creates a highly innovative material with the potential to achieve the long-sought goal of long-term, cyclic high-temperature use of C/C in an oxidizing environment. The C/C substructure provided most of the mechanical integrity, and the CMC strengths achieved appeared to be sufficient to allow the CMC to perform its primary function of protecting the C/C.

Nozzle extension components were fabricated and successfully hot-fire tested. Test results showed good thermochemical and thermomechanical stability of the CMC, as well as excellent interfacial bonding between the CMC liner and the underlying C/C structure. In particular, hafnium-containing CMCs on C/C were shown to perform well at temperatures exceeding 3,500 °F (≈1,925 °C).

The melt-infiltrated CMC-lined C/C composites offered a lower density than Cf/SiC. The melt-infiltrated composites offer greater use temperature than Cf/SiC because of the more refractory ceramic matrices and the C/C substructure provides greater high-temperature strength.

The progress made in this work will allow multiple high-temperature components used in oxidizing environments to take advantage of the low density and high strength of C/C combined with the high-temperature oxidation resistance of melt-infiltrated CMCs.

This work was done by Matthew J. Wright, Gautham Ramachandran, and Brian E. Williams of Ultramet for Glenn Research Center. Further information is contained in a TSP (see page 1).

Inquiries concerning rights for the commercial use of this invention should be addressed to NASA Glenn Research Center, Innovative Partnerships Office, Attn: Steven Fedor, Mail Stop 4-8, 21000 Brookpark Road, Cleveland, Ohio 44135. Refer to LEW-18618-1.



Sample Acquisition and Handling System From a Remote Platform

This technology can be used for surface sampling of large areas such as deserts, or for agricultural sampling.

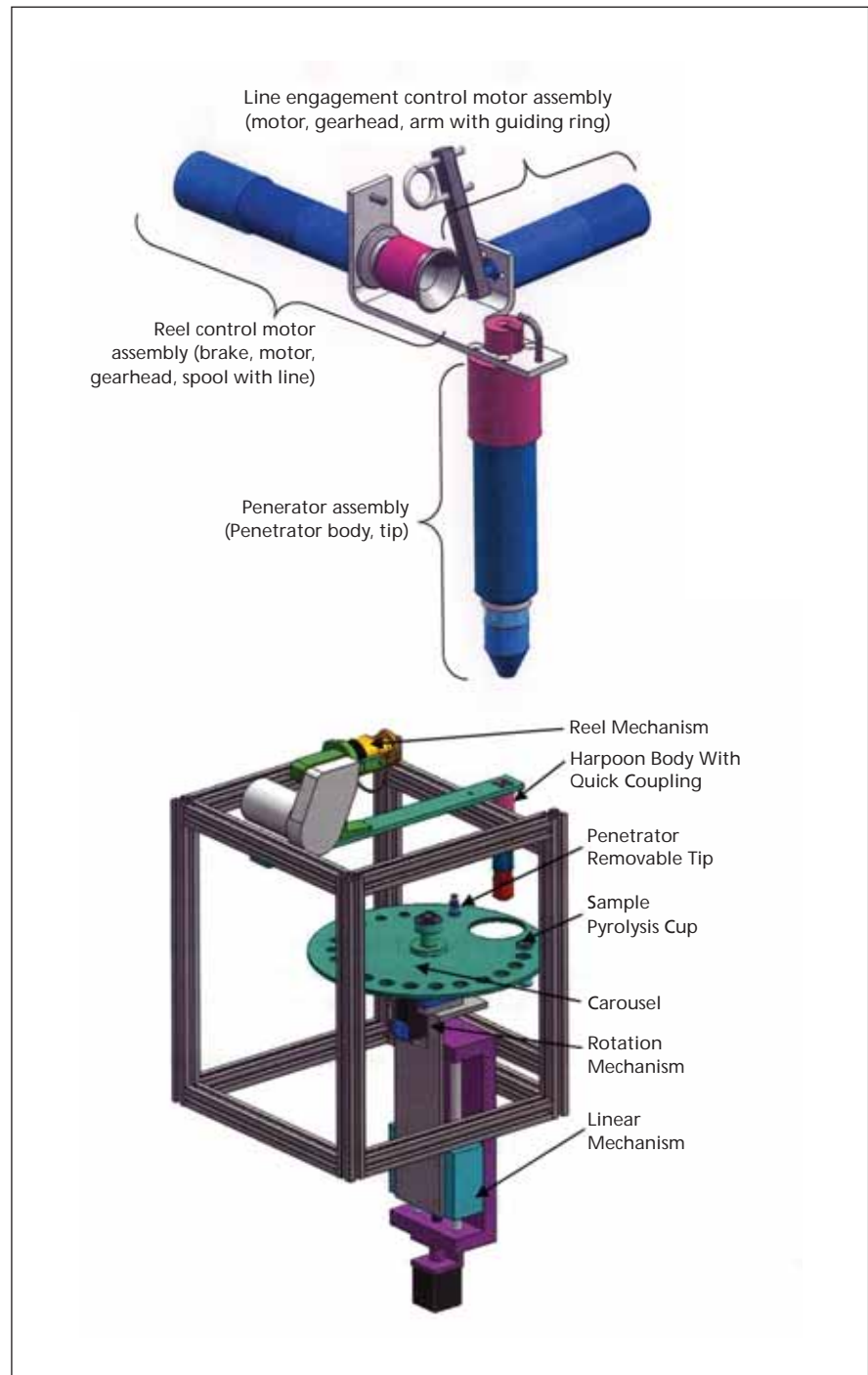
NASA's Jet Propulsion Laboratory, Pasadena, California

A system has been developed to acquire and handle samples from a suspended remote platform. The system includes a penetrator, a penetrator deployment mechanism, and a sample handler. A gravity-driven harpoon sampler was used for the system, but other solutions can be used to supply the penetration energy, such as pyrotechnic, pressurized gas, or springs. The deployment mechanism includes a line that is attached to the penetrator, a spool for reeling in the line, and a line engagement control mechanism.

The penetrator has removable tips that can collect liquid, ice, or solid samples. The handling mechanism consists of a carousel that can store a series of identical or different tips, assist in penetrator reconfiguration for multiple sample acquisition, and deliver the sample to a series of instruments for analysis. The carousel sample handling system was combined with a brassboard reeling mechanism and a penetrator with removable tips. It can attach the removable tip to the penetrator, release and retrieve the penetrator, remove the tip, and present it to multiple instrument stations. The penetrator can be remotely deployed from an aerobot, penetrate and collect the sample, and be retrieved with the sample to the aerobot.

The penetrator with removable tips includes sample interrogation windows and a sample retainment spring for unconsolidated samples. The line engagement motor can be used to control the penetrator release and reeling engagement, and to evenly distribute the line on the spool by rocking between left and right ends of the spool. When the arm with the guiding ring is aligned with the spool axis, the line is free to unwind from the spool without rotating the spool. When the arm is perpendicular to the spool axis, the line can move only if the spool rotates.

This work was done by Mircea Badescu, Stewart Sherrit, and Jack A. Jones of Caltech for NASA's Jet Propulsion Laboratory. Further information is contained in a TSP (see page 1). NPO-46585



The main functional components of the Penetrator Deployment Mechanism (top), and (bottom) the Brassboard with a simplified sample acquisition component and the carousel sample handler.

⚙ Improved Rare-Earth Emitter Hollow Cathode

These cathodes have applications in electric thrusters and in industry for plasma processing of optical coatings.

NASA's Jet Propulsion Laboratory, Pasadena, California

An improvement has been made to the design of the hollow cathode geometry that was created for the rare-earth electron emitter described in "Compact Rare Earth Emitter Hollow Cathode" (NPO-44923), *NASA Tech Briefs*, Vol. 34, No. 3 (March 2010), p. 52. The original interior assembly was made entirely of graphite in order to be compatible with the LaB₆ material, which cannot be touched by metals during operation due to boron diffusion causing embrittlement issues in high-temperature refractory materials. Also, the graphite tube was difficult to machine and was subject to vibration-induced fracturing.

This innovation replaces the graphite tube with one made out of refractory metal that is relatively easy to manufacture. The cathode support tube is made

of molybdenum or molybdenum-rhenium. This material is easily gun-bored to near the tolerances required, and finish machined with steps at each end that capture the orifice plate and the mounting flange. This provides the manufacturability and robustness needed for flight applications, and eliminates the need for expensive e-beam welding used in prior cathodes. The LaB₆ insert is protected from direct contact with the refractory metal tube by thin, graphite sleeves in a cup-arrangement around the ends of the insert. The sleeves, insert, and orifice plate are held in place by a ceramic spacer and tungsten spring inserted inside the tube.

To heat the cathode, an insulating tube is slipped around the refractory metal hollow tube, which can be made

of high-temperature materials like boron nitride or aluminum nitride. A screw-shaped slot, or series of slots, is machined in the outside of the ceramic tube to constrain a refractory metal wire wound inside the slot that is used as the heater. The screw slot can hold a single heater wire that is then connected to the front of the cathode tube by tack-welding to complete the electrical circuit, or it can be a double slot that takes a bifilar wound heater with both leads coming out the back. This configuration replaces the previous sheathed heater design that limited the cycling-life of the cathode.

This work was done by Dan M. Goebel of Caltech for NASA's Jet Propulsion Laboratory. Further information is contained in a TSP (see page 1). NPO-46782

⚙ High-Temperature Smart Structures for Engine Noise Reduction and Performance Enhancement

The most direct beneficiary of this hardware would be next-generation subsonic transports.

John H. Glenn Research Center, Cleveland, Ohio

One of key NASA goals is to develop and integrate noise reduction technology to enable unrestricted air transportation service to all communities. One of the technical priorities of this activity has been to account for and reduce noise via propulsion/airframe interactions, identifying advanced concepts to be integrated with the airframe to mitigate these noise-producing mechanisms.

An adaptive geometry chevron using embedded smart structures technology offers the possibility of maximizing engine performance while retaining and possibly enhancing the favorable noise characteristics of current designs. New high-temperature shape memory alloy (HTSMA) materials technology enables the devices to operate in both low-temperature (fan) and high-temperature (core) exhaust flows. Chevron-equipped engines have demonstrated reduced noise in testing and operational use. It is desirable to have the noise benefits of chevrons in takeoff/landing conditions, but have them deployed into a mini-

mum drag position for cruise flight.

The central feature of the innovation was building on rapidly maturing HTSMA technology to implement a next-generation aircraft noise mitigation system centered on adaptive chevron flow control surfaces. In general, SMA-actuated devices have the potential to enhance the demonstrated noise reduction effectiveness of chevron systems while eliminating the associated performance penalty. The use of structurally integrated smart devices will minimize the mechanical and subsystem complexity of this implementation.

The central innovations of the effort entail the modification of prior chevron designs to include a small cut that relaxes structural stiffness without compromising the desired flow characteristics over the surface; the reorientation of SMA actuation devices to apply forces to deflect the chevron tip, exploiting this relaxed stiffness; and the use of high-temperature SMA (HTSMA) materials to enable operation in the de-

manding core chevron environment.

The overall conclusion of these design studies was that the cut chevron concept is a critical enabling step in bringing the variable geometry core chevron within reach. The presence of the cut may be aerodynamically undesirable in some respects, but it is present only when the chevron is not immersed in the core jet exhaust. When deployed, the gap closes as the chevron tip enters the high-speed, high-temperature core stream. Aeroacoustic testing and flow visualization support the contention that this cut is inconsequential to chevron performance.

This work was done by Todd R. Quackenbush and Robert M. McKillip, Jr., of Continuum Dynamics, Inc. for Glenn Research Center.

Inquiries concerning rights for the commercial use of this invention should be addressed to NASA Glenn Research Center, Innovative Partnerships Office, Attn: Steve Fedor, Mail Stop 4-8, 21000 Brookpark Road, Cleveland, Ohio 44135. Refer to LEW-18416-1

⚙️ Cryogenic Scan Mechanism for Fourier Transform Spectrometer

This mechanism would be applicable to FTS use in forensic, scientific, medical, and defense industries.

Goddard Space Flight Center, Greenbelt, Maryland

A compact and lightweight mechanism has been developed to accurately move a Fourier transform spectrometer (FTS) scan mirror (a cube corner) in a near-linear fashion with near constant speed at cryogenic temperatures. This innovation includes a slide mechanism to restrict motion to one dimension, an actuator to drive the motion, and a linear velocity transducer (LVT) to measure the speed. The cube corner mirror is double-passed in one arm of the FTS; double-passing is required to compensate for optical beam shear resulting from tilting of the moving cube corner.

The slide, actuator, and LVT are off-the-shelf components that are capable

of cryogenic vacuum operation. The actuator drives the slide for the required travel of 2.5 cm. The LVT measures translation speed. A proportional feedback loop compares the LVT voltage with the set voltage (speed) to derive an error signal to drive the actuator and achieve near constant speed. When the end of the scan is reached, a personal computer reverses the set voltage.

The actuator and LVT have no moving parts in contact, and have magnetic properties consistent with cryogenic operation. The unlubricated slide restricts motion to linear travel, using crossed roller bearings consistent with 100-mil-

lion-stroke operation. The mechanism tilts several arc seconds during transport of the FTS mirror, which would compromise optical fringe efficiency when using a flat mirror. Consequently, a cube corner mirror is used, which converts a tilt into a shear. The sheared beam strikes (at normal incidence) a flat mirror at the end of the FTS arm with the moving mechanism, thereby returning upon itself and compensating for the shear.

This work was done by John C. Brasunas and John J. Francis of Goddard Space Flight Center. For further information, contact the Goddard Innovative Partnerships Office at (301) 286-5810. GSC-15556-1

⚙️ Piezoelectric Rotary Tube Motor

NASA's Jet Propulsion Laboratory, Pasadena, California

A custom rotary SQUIGGLE[®] motor has been developed that sets new benchmarks for small motor size, high position resolution, and high torque without gear reduction. Its capabilities cannot be achieved with conventional electromagnetic motors. It consists of piezoelectric plates mounted on a square flexible tube. The plates are actuated via voltage waveforms 90° out of phase at the reso-

nant frequency of the device to create rotary motion.

The motors were incorporated into a two-axis positioner that was designed for fiber-fed spectroscopy for ground-based and space-based projects. The positioner enables large-scale celestial object surveys to take place in a practical amount of time.

This work was done by Charles D. Fisher, Mircea Badescu, and David F. Braun of Cal-

tech and Rob Culhane of New Scale Technologies for NASA's Jet Propulsion Laboratory. For more information about the motor and the positioner, visit the following sites:

http://www.newscaletech.com/custom_overview.html#rotary

http://www.newscaletech.com/app_notes/7Cobra-JPL-article.html

NPO-46992



Thermoelectric Energy Conversion Technology for High-Altitude Airships

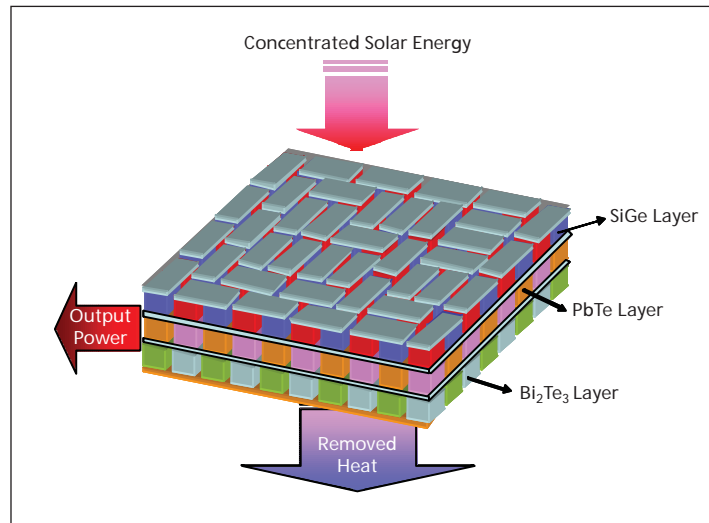
Applications include surveillance for homeland security, and Earth observation for weather monitoring.

Langley Research Center, Hampton, Virginia

The High Altitude Airship (HAA) has various application potential and mission scenarios that require onboard energy harvesting and power distribution systems. The power technology for HAA maneuverability and mission-oriented applications must come from its surroundings, e.g. solar power. The energy harvesting system considered for HAA is based on the advanced thermoelectric (ATE) materials being developed at NASA Langley Research Center. The materials selected for ATE are silicon germanium (SiGe) and bismuth telluride (Bi_2Te_3), in multiple layers. The layered structure of the

advanced TE materials is specifically engineered to provide maximum efficiency for the corresponding range of operational temperatures. For three layers of the advanced TE materials that operate at high, medium, and low temperatures, correspondingly in a tandem mode, the cascaded efficiency is estimated to be greater than 60 percent.

The first layer is built from the array of SiGe, while the second and third layers are respectively built from PbTe and



The ATE Energy Conversion Device consists of triple layers of p-n-junction arrays in a tandem mode. The first layer is built from the array of SiGe, while the second and third layers are built from PbTe and Bi_2Te_3 , respectively, as regenerative cycles. Such an arrangement allows effective energy harvesting from a heat source.

Bi_2Te_3 as regenerative cycles. Such an arrangement allows effective energy harvesting from a heat source. First, solar flux is concentrated and heats up the first layer, which is built with high-temperature SiGe. The unused thermal energy from the first layer is subsequently used by the second layer, which is built with mid-temperature PbTe. The third layer of Bi_2Te_3 uses the unused energy from the second layer to maximize the conversion of the energy that is other-

wise dumped away. In this fashion, the ATE devices become more effective than solar cells because the performance of solar cells is monolithically tied to band-gap energy structure, so that they only couple with certain spectral lines.

For nighttime, the power required must be augmented from the onboard fuel cells, battery, and a rectenna array that is attached at the bottom surface of HAA. These systems combined provide at least a megawatt level of power for the intermittent operation.

Commercial applications include monitoring and controlling the ever-increasing complexities of aerial

and maritime transportation and telecommunication networks. Military applications include close and persistent surveillance of adversarial elements, possibly controlling enemy infiltrations through open air and sea and shooting down enemy missiles during their boosting phase.

This work was done by Sang H. Choi, James R. Elliott, Glen C. King, Yeonjoon Park, Jae-Woo Kim, and Sang-Hyon Chu of Langley Research Center. Further information is contained in a TSP (see page 1). LAR-17213-1

Combustor Computations for CO₂-Neutral Aviation

This method can be used to determine synthetic and biological fuels and blends.

John H. Glenn Research Center, Cleveland, Ohio

Knowing the pure component C_p^0 or mixture C_p^0 as computed by a flexible code such as NIST-STRAPP or McBride-Gordon, one can, within reasonable accuracy, determine the thermophysical properties

necessary to predict the combustion characteristics when there are no tabulated or computed data for those fluid mixtures or limited results for lower temperatures. (Note: C_p^0 is molar heat capacity at con-

stant pressure.) The method can be used in the determination of synthetic and biological fuels and blends using the NIST code to compute the C_p^0 of the mixture.

In this work, the values of the heat ca-

capacity were set at "zero" pressure, which provided the basis for integration to determine the required combustor properties from the injector to the combustor exit plane. The McBride-Gordon code was used to determine the heat capacity at zero pressure over a wide range of temperatures (room to 6,000 K). The selected fluids were Jet-A, 224TMP (octane), and C12. It was found that each heat capacity loci were form-similar. It was then determined that the results [near 400 to 3,000 K] could be represented to within acceptable engineering accuracy with the simplified equation $C_p^0 = A/T + B$, where A and B are fluid-dependent constants and T is temperature (K).

With this information, a model for JP8 was established using NIST Code STRAPP with a 12-component mixture. Selected pure components such as C12 and 224TMP have representations in both the

McBride-Gordon and NIST codes, and were calculated and compared. A 12-component mixture was defined for JP8 and C_p^0 computed using the NIST code to 1,000 K. The simplified representation of the C_p^0 for JP8 was form-similar to Jet-A, C12, and 224TMP over the range of 400 to 3,000 K. This defined the ability to predict the C_p^0 for a variety of hydrocarbon mixtures using the NIST code to 1,000 K, and representing these data by the simplified C_p^0 , which can then be extrapolated to 3,000 K within reasonable engineering accuracy. Knowing $C_p^0(T)$ results for enthalpy, entropy, and free energy can be determined and input into the combustion code.

The simplified form of the gas phase caloric equations generated using the NIST STRAPP code, the NASA McBride code, and a systematic curve-fitting methodology, work well within an established computational fluid dynamics (CFD) flow solver. Computed flow struc-

ture for the four fuels, using a trapped vortex combustor experimental rig as a test case, show strong similarities. This is true for the temperature as well as the CO and CO₂ mass fraction contours. Inspection of the mass-averaged combustor exit quantities, however, indicates that temperature differences may be sufficient to require reconsideration of turbine fueling schemes.

This work was done by Robert C. Hendricks of Glenn Research Center; Andreja Brankovic and Robert C. Ryder of Flow Parametrics; and Marcia Huber of the National Institute of Standards and Technology. Further information is contained in a TSP (see page 1).

Inquiries concerning rights for the commercial use of this invention should be addressed to NASA Glenn Research Center, Innovative Partnerships Office, Attn: Steve Fedor, Mail Stop 4-8, 21000 Brookpark Road, Cleveland, Ohio 44135. Refer to LEW-18453-1.



Use of Dynamic Distortion to Predict and Alleviate Loss of Control This work alleviates aircraft loss due to unfavorable pilot/vehicle interactions.

Dryden Flight Research Center, Edwards, California

This research has developed and evaluated the specific concepts, termed “Smart-Cue” and “Smart-Gain,” to alleviate aircraft loss of control that results from unfavorable pilot/vehicle system interactions, including pilot-induced oscillations (PIOs). Unfavorable pilot/vehicle-system interactions have long been an aviation safety problem. While the effective aircraft dynamic properties involved in these events have been extensively studied and understood, similar scrutiny has not been paid to the many aspects of the primary manual control system that converts the pilot control inputs to motions of the control surfaces. The purpose of the Smart-Cue and Smart-Gain developments is to redress this neglect, and to develop and validate remedial manual control systems.

The program began with a review of the historical precedent for providing cueing to the pilot via the cockpit controls along with the many control surface rate-limiting alleviation schemes and PIO suppression filter concepts that have been proposed and evaluated over the years. A McFadden hydraulic control

loader capable of generating proposed Smart-Cue forces was integrated with the STI PC-based flight simulator. Candidate mechanizations of the Smart-Cue concept were created, implemented, assessed, and refined through a series of evaluations using guest test pilots. The Smart-Gain concept was developed in response to the Smart-Cue performance during the precision offset landings conducted during the checkout flights. Rapid prototyping of the Smart-Gain mechanization was made via the piloted simulation, and the concept was included as part of the formal flight test evaluations. Five test pilots participated in the Smart-Cue/Smart-Gain evaluations with the Learjet in-flight simulator.

In this work, the “distortion” of interest results from control surface rate-limiting, and is quantified by the surface Position Error, while the “distortion metric” is the Position Lag. A force feedback cue, the constraining function, and/or a command path gain reduction, are created when the Position Error exceeds the Position Lag, or the alerting function. The overall imple-

mentation does, however, require hardware in the form of a back-driven force-feel system included as part of the cockpit manipulator. The feasibility of the Smart-Cue/Smart-Gain approach using a back-driven manipulator implemented in a variable stability aircraft was successfully demonstrated in flight.

The hypothesis stated that the Smart-Cue will change pilot behavior to decrease the chance of adverse pilot/vehicle system interactions. Thus, if this assumption about the pilot-vehicle system was found to be true, then a degraded flight-control system in the presence of dynamic distortions will have improved stability and performance. This hypothesis was found to be true in flight-testing evaluations that replicated high-gain, continuous closed-loop tasks for both cruise and terminal flight operations, especially for those cases that included the addition of the Smart-Gain.

This work was done by David Klyde, Chi-Ying Liang, and Daniel Alvarez of Systems Technology, Inc. for Dryden Flight Research Center. Further information is contained in a TSP (see page 1). DRC-007-083

Cycle Time Reduction in Trapped Mercury Ion Atomic Frequency Standards

NASA's Jet Propulsion Laboratory, Pasadena, California

The use of the mercury ion isotope $^{201}\text{Hg}^+$ was examined for an atomic clock. Taking advantage of the faster optical pumping time in $^{201}\text{Hg}^+$ reduces both the state preparation and the state readout times, thereby decreasing the overall cycle time of the clock and reducing the impact of medium-term LO noise on the performance of the frequency standard. The spectral overlap between the plasma discharge lamp used for $^{201}\text{Hg}^+$ state preparation and readout is much larger than that of the lamp used for the more conventional $^{199}\text{Hg}^+$. There has been little study of $^{201}\text{Hg}^+$ for clock applications (in fact,

all trapped ion clock work in mercury has been with $^{199}\text{Hg}^+$); however, recently the optical pumping time in $^{201}\text{Hg}^+$ has been measured and found to be 0.45 second, or about three times faster than in $^{199}\text{Hg}^+$ due largely to the better spectral overlap. This can be used to reduce the overall clock cycle time by over 2 seconds, or up to a factor of 2 improvement.

The use of the $^{201}\text{Hg}^+$ for an atomic clock is totally new. Most attempts to reduce the impact of LO noise have focused on reducing the interrogation time. In the trapped ion frequency standards built so far at JPL, the optical

pumping time is already at its minimum so that no enhancement can be had by shortening it. However, by using $^{201}\text{Hg}^+$, this is no longer the case. Furthermore, integrity monitoring, the mechanism that determines whether the clock is functioning normally, cannot happen faster than the clock cycle time. Therefore, a shorter cycle time will enable quicker detection of failure modes and recovery from them.

This work was done by Eric A. Burt, Robert L. Tjoelker, and Shervin Taghavi of Caltech for NASA's Jet Propulsion Laboratory. For more information, contact iaoffice@jpl.nasa.gov. NPO-46865

A²⁰¹Hg⁺ Comagnetometer for ¹⁹⁹Hg⁺ Trapped Ion Space Atomic Clocks

NASA's Jet Propulsion Laboratory, Pasadena, California

A method has been developed for unambiguously measuring the exact magnetic field experienced by trapped mercury ions contained within an atomic clock intended for space applications. In general, atomic clocks are insensitive to external perturbations that would change the frequency at which the clocks operate. On a space platform, these perturbative effects can be much larger than they would be on the ground, especially in dealing with the magnetic field environment. The solution is to use a different isotope of mercury held within the same trap as the clock isotope. The magnetic field can be very accurately measured with a magnetic-field-sensitive atomic transition in

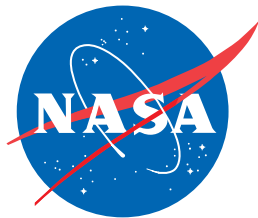
the added isotope. Further, this measurement can be made simultaneously with normal clock operation, thereby not degrading clock performance.

Instead of using a conventional magnetometer to measure ambient fields, which would necessarily be placed some distance away from the clock atoms, first-order field-sensitive atomic transition frequency changes in the atoms themselves determine the variations in the magnetic field. As a result, all ambiguity over the exact field value experienced by the atoms is removed. Atoms used in atomic clocks always have an atomic transition (often referred to as the "clock transition") that is sensitive to magnetic fields only in second order,

and usually have one or more transitions that are first-order field sensitive. For operating parameters used in the ¹⁹⁹Hg⁺ clock, the latter can be five orders of magnitude or more sensitive to field fluctuations than the clock transition, thereby providing an unambiguous probe of the magnetic field strength.

This work was done by Eric A. Burt, Shervin Taghavi, and Robert L. Tjoelker of Caltech for NASA's Jet Propulsion Laboratory. For more information, contact iaoffice@jpl.nasa.gov.

This invention is owned by NASA, and a patent application has been filed. Inquiries concerning nonexclusive or exclusive license for its commercial development should be addressed to the Patent Counsel, NASA Management Office–JPL. Refer to NPO-46938.



National Aeronautics and
Space Administration